applied sciences

MDPI

Article

Structural, Morphological, and Electrochemical Performance of CeO_2/NiO Nanocomposite for Supercapacitor Applications

Naushad Ahmad [1], Abdulaziz Ali Alghamdi [1], Hessah A. AL-Abdulkarim [1], Ghulam M. Mustafa [2], Neazar Baghdadi [3] and Fahad A. Alharthi [1,*]

[1] Department of Chemistry, College of Science, King Saud University, Riyadh 11451, Saudi Arabia; anaushad@ksu.edu.sa (N.A.); aalghamdia@ksu.edu.sa (A.A.A.); hessah@ksu.edu.sa (H.A.A.-A.)
[2] Department of Physics, The University of Lahore, Lahore 54590, Pakistan; ghulam.mustafa@phys.uol.edu.pk
[3] Center of Nanotechnology, King Abdulaziz University, Jeddah 80200, Saudi Arabia; nebaghdadi@kau.edu.sa
* Correspondence: fharthi@ksu.edu.sa

Abstract: The composite of ceria has been widely studied as an electrode material for supercapacitors applications due to its high energy density. Herein, we synthesize CeO_2/NiO nanocomposite via a hydrothermal route and explore its different aspects using various characterization techniques. The crystal structure is investigated using X-ray diffraction, Fourier transform infrared, and Raman spectroscopy. The formation of nanoflakes which combine to form flower-like morphology is observed from scanning electron microscope images. Selected area scans confirm the presence of all elements in accordance with their stoichiometric amount and thus authenticate the elemental purity. Polycrystalline nature with crystallite size 8–10 nm having truncated octahedron shape is confirmed from tunneling electron microscope images. Using X-ray photoelectron spectroscopy the different oxidation states of Ce and Ni are observed which play the role of active sites in the electrochemical performance of this nanocomposite material. Cyclic Voltammetry(CV) measurements at different scan rates and Galvanic Charge Discharge (GCD) measurements at different current densities are performed to probe the electrochemical response which revealed the potential of CeO_2/NiO nanocomposite as an electrode material for energy storage devices.

Keywords: CeO_2/NiO nanocomposite; electrode materials; supercapacitor; energy density; power density

Citation: Ahmad, N.; Ali Alghamdi, A.; AL-Abdulkarim, H.A.; Mustafa, G.M.; Baghdadi, N.; Alharthi, F.A. Structural, Morphological, and Electrochemical Performance of CeO_2/NiO Nanocomposite for Supercapacitor Applications. *Appl. Sci.* **2021**, *11*, 411. https://doi.org/10.3390/app11010411

Received: 22 November 2020
Accepted: 30 December 2020
Published: 4 January 2021

1. Introduction

An emerging device for storing and converting energy, the supercapacitor has been used in place of batteries and conventional capacitors. They possess many advantages and potential due to various reasons. They exhibit high power density and great efficiencies along with a high capability of charge/discharge and long cyclic stability [1]. There are many applications of supercapacitors in different fields that include auto-motives and portable electronic devices as well as aerospace and military fields and many more. Mainly, supercapacitors are categorized into two types. First, is electric double-layer capacitors (EDLCs) and the second is pseudocapacitors (PCs). The EDLCs have higher values of capacitance in contrast with conventional capacitors due to the short distance up to the nanometer level between the double layers [2]. The ability of charge storage in EDLCs on the surface of electrode materials depends upon the adsorption and desorption of electrolyte ions. Despite the high reversibility and perfect cyclic performance of EDLCs, their energy density is still low which limits their applications. The other form of supercapacitors, PCs, can store charge on the surface of the electrode material having fast faradaic redox reactions and rely on high reversibility confirming the battery-like nature [3,4]. The electrolyte ions that cause fast faradaic reactions can be inserted and deserted on the interfaces between electrolyte and electrode. The specific capacitance of PCs is greater than EDLCs. Commonly used electrode materials in PCs are oxides, sulfides, hydroxides, and phosphides of transition metals. We synthesized this nanocomposite using oxides of nickel

and cerium. The properties of EDLCs and PCs can be combined in hybrid supercapacitors (HSCs) in which negative electrode materials are made up of carbon materials while positive electrode materials are composed of battery-like transition metal oxides (TMOs) [5,6]. This approach also enhances the potential window or the working voltage range of the device. This increase in the potential window is directly linked with the energy density of the electrode material which is measured using: $E = \frac{1}{2} CV^2$. In the recent decade, a lot of work has been devoted to the positive electrode materials that have high energy density, specific capacitances, and are eco-friendly [7–9].

Rare earth metal oxide, cerium oxide, is an intensively studied material because of its vast applications such as in portable devices, electrical vehicles, and sustainable energy devices. The composite of cerium oxide can be used for catalytic redox reactions and to clean the exhaust of automobiles. The reversible chemical reaction depends upon the chemical potential of oxygen between the two cerium oxides that can cause a catalytic effect. These two cerium oxides are oxygen-poor Ce_2O_3 and oxygen-rich CeO_2. To expand the catalytic process of cerium oxide it is much needed to find novel metal ions that can be doped in CeO_2 which can further improve the oxygen storage capacity [10,11]. In this regard, researchers working across the globe have attempted to mix the oxides of rare-earth metals, transition metals, and alkaline metals with Ce sub-lattice. To compensate charges in the lattice, the anion vacancy sites can be created by changing Ce^{4+} with Ce^{2+} and Ce^{3+} cations which leads to enhance the ionic conductivity for oxygen. However, the doping is carried out under dopant selection criteria i.e., the ionic radius of dopant must be comparable to the ionic radius of the host [12].

From the literature, it is noticed that the addition of transition metal ions is suitable for doping in CeO_2. Generally, the composites of CeO_2 with Cu doping represent enhanced catalytic performances as well as high oxygen storage capacities and high specific surface areas [13]. Some salient features of CeO_2 which make it a potential material for various industrial applications include: (i) exceptional mechanical strength and high transmission, (ii) high oxygen storage capacity and high conductivity, (iii) high specific surface area and good redox performances, (iv) thermally stable at high temperatures and have abundant active sites, and (v) have a lot of oxygen vacancies on the surface. All these properties can further be improved by making composite or doping of metals or metal oxides in ceria. Various transition metal oxides such as zinc oxide, manganese oxide, nickel oxide, titanium oxide, and copper oxide have been doped in ceria to enhance its performance [14].

The composites of cerium oxide have potential applications such as electrochemical sensors, photo-catalyst as well as in energy storage systems and supercapacitors. Ahmed et al. [15] used the solution combustion route to synthesize the nanocomposite of NiO/CeO_2 where they used metal nitrates as oxidizers and glycine as fuel. Different characterization techniques including XRD, TEM, and FTIR were used to investigate structural along with morphological and surface characteristics of this nanocomposite. Their results revealed that these compositions were suitable for electrochemical systems and can be used as electrodes due to their reproducibility as well as electrocatalytic activity and stability. The same group of researchers [16] doped ZnO in cerium oxide via a microwave-assisted method and confirmed the crystalline structure of composites with a high density of particles. Ansari et al. [17] investigated the physiochemical characteristics of the nanocomposite of CeO_2 by doping Cu in it. By increasing the doping concentration of Cu, band gap energies were increased which is an indication of the production of oxygen vacancies. These compositions can be utilized as electrode material for fuel cells and electrochemical systems as they can be operated at low temperatures up to 162 °C [18].

In the present work, we synthesized nanocomposites of NiO/CeO_2 via hydrothermal route and investigated their structural, microstructural, morphological, optical, and electrochemical properties in detail which witnessed the importance of nanocomposites as an electrode material for energy storage devices.

2. Experimental

2.1. Synthesis of CeO_2/NiO Nanocomposite

The nanocomposite of different metal oxides with ceria can be made using different chemical methods like ball milling, co-precipitation, sol-gel auto-combustion, and the hydrothermal method. Among these available methods, we adopted the hydrothermal method to synthesize the NiO/CeO_2 nanocomposite. For this purpose, the weighted amounts of nitrates of Ni and Ce were dissolved in 50 mL distilled water and then the fuel agent, glycine, was put into the solution of nitrates. In order to keep the pH at 10, 1M solution of NaOH was put drop-wise in the solution and stirred continuously. This stirring was continued for an hour. After that, this solution was shifted into a Teflon-lined autoclave made of stainless steel which was placed in an oven at 150 °C for 12 h for hydrothermal reaction to occur. Furthermore, the autoclave was cooled to room temperature (RT) and the resultant precipitates were filtered. These precipitates were washed several times with DI water and ethanol. After washing, these precipitates were dried at 80 °C for 24 h. Lastly, the obtained powder was calcined at 550 °C for 5 h [19].

2.2. Characterization Techniques

The structural investigation was carried out using Bruker D8 advanced diffractometer with Cu Kα radiation having λ = 0.1540 nm. This pattern was recorded in the 2θ range of 20 to 75 degrees. The structure was further analyzed using Raman spectroscopy. The morphological analysis was done by JOEL JSM-7600F scanning electron microscopy (SEM) and then elemental analysis was done with the help of energy-dispersive X-ray spectroscopy (EDX). An accelerating voltage of 20 kV was set for EDX. The surface chemical compositions were investigated using X-ray photoelectron spectroscopy (XPS). CS350 potentiostat was used to record the CV loops at different scan rates (0.005, 0.01, 0.05, and 0.1 mVs^{-1}) in the potential window 0–0.5 V. Using the same instrument, charge/discharge curves and impedance measurements were also recorded [20,21].

2.3. Fabrication of Supercapacitor Electrode and Electrochemical Tests

All electrochemical experiments were performed on a CHI 601C Electrochemical Workstation (CH Instrument, Austin, TX, USA), using a traditional three-electrode electrochemical cell (a working volume of 5 mL) with a working electrode, an Ag/AgCl (saturated KCl) reference electrode, and a platinum wire counter electrode. The working electrode was prepared by mixing active material with carbon black (conductive agent) and polyvinylidene fluoride (PVDF) (binder) with a mass ratio of 8:1:1 using ethanol as solvent. The mixture was cast onto Ni foam with an area of 1 cm^2 and a weight of about 1 mg. The electrode was dried at 60 °C overnight before the test. 3M KOH was used as the electrolyte. The synthesis summary of electrode preparation is shown in Figure 1.

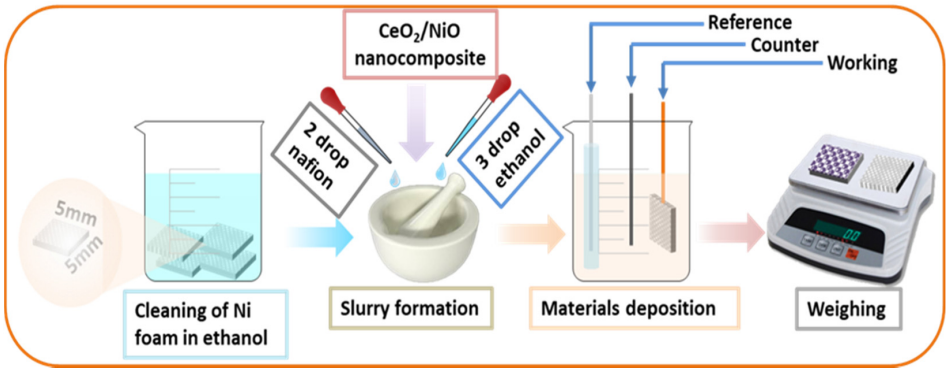

Figure 1. A schematic of electrode synthesis.

3. Results and Discussion

XRD is a powerful technique that is extensively used to study the crystal structure, lattice parameters, crystallite size, dislocation density as well as crystal strain. The development of a particular crystalline phase was critically governed by the calcination process. Figure 2 shows the XRD pattern of CeO_2/NiO nanocomposite in the 2θ range of 20–75 degrees. The diffracted peaks appearing at 2θ values of 28.7° and 47.4° were indexed as (111) and (220) and matched with the ICSD ref. no. 00-001-0800 which confirmed the presence of CeO_2 while peaks appearing at 33.1°, 56.4°, 62.3°, and 69.8° were indexed as (200), (311), (103), and (440) and matched with ICSD ref. no. 01-073-1519 which confirmed the presence of the NiO phase having an FCC structure [22]. Since there was no peak other than CeO_2 and NiO, it confirmed the formation of CeO_2/NiO nanocomposite. For CeO_2, the most intense peak was (111) and for NiO, it was (200). Using Scherrer's formula, the crystallite size was calculated from the most intense peaks. The calculated crystallite size was ~10 nm for CeO_2 and 15 nm for NiO.

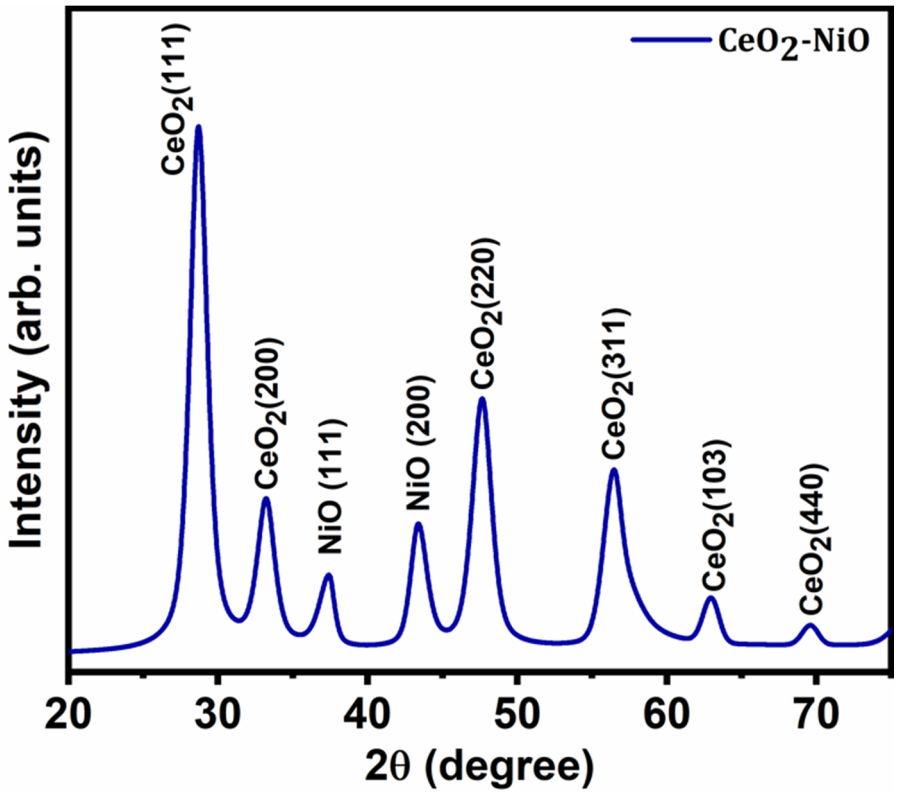

Figure 2. Indexed XRD pattern of CeO_2/NiO nanocomposite.

Figure 3 shows the SEM images of CeO_2/NiO nanocomposite at (a) 4000 and 50,000 magnifications from where we can analyze the morphology, particle size distribution, and surface texture. The image at low magnification (Figure 3a) covered more area and thus provided useful information regarding particle distribution which was uniform throughout the surface. When magnification was increased (Figure 3b), it provided more chance to look into the minor details and thus revealed a cauliflower's leaf-like morphology. This kind of morphology exposed high surface area and thus had high potential as an electrode material for energy storage devices like supercapacitors [23].

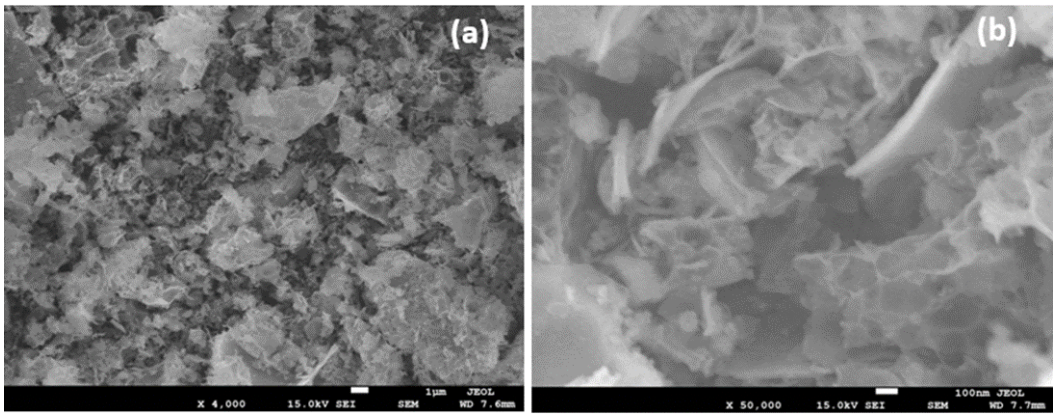

Figure 3. SEM images of CeO_2/NiO nanocomposite at (**a**) 4000× and (**b**) 50,000×.

To check the elemental composition of the prepared sample, EDX analysis was performed at a fixed area of SEM images as shown in Figure 4. The purity of the sample could be verified from the EDX spectra because there were only peaks of Ce, Ni, and O in the graph with wt. % of 44.80, 23.08, and 25.84, respectively. In addition, a peak of C was also there in the low energy region which came from the environment. The weight percentages of all these elements were provided in the tabular form as an inset.

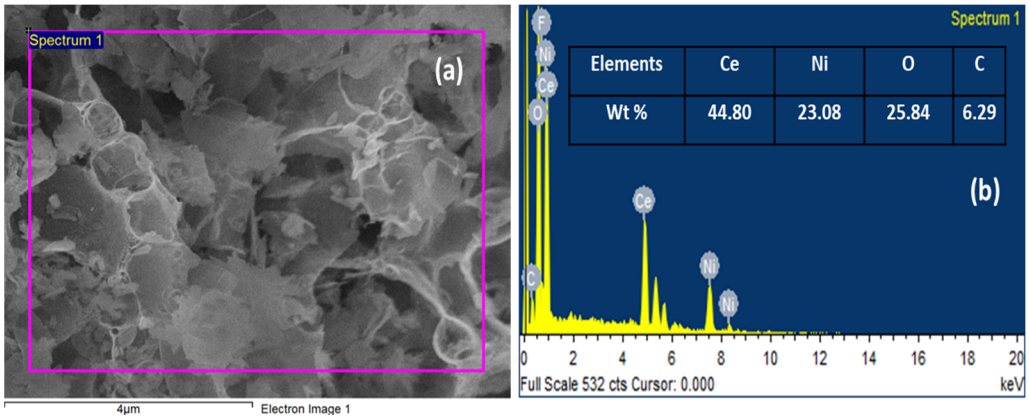

Figure 4. (**a**) SEM image of CeO_2/NiO nanocomposite with scan area and (**b**) Energy-dispersive X-ray spectroscopy (EDX) spectrum with a weight percentage of all elements.

In order to reveal the minor details of morphology and crystal geometry, the HR-TEM images were captured as shown in Figure 5. Figure 5a,b revealed the polycrystalline nature of this nanocomposite with the interplanar spacing of 0.155 nm. Some of these crystallites were grown in bipyramid shape as highlighted by sketching its schematic. The presence of concentric circles shown in the SEAD pattern supported the polycrystalline nature (Figure 5c). Here, the estimated value of crystallite size was in good agreement with the XRD results [24].

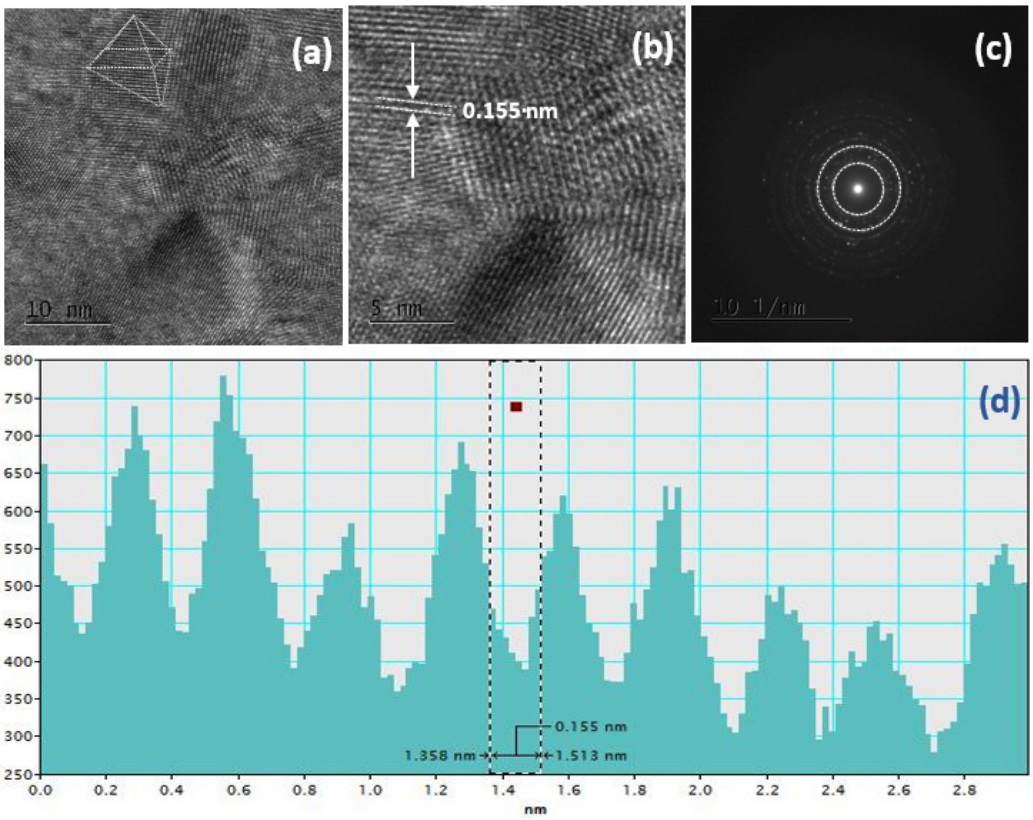

Figure 5. (**a**,**b**) HR-TEM images, (**c**) SEAD pattern, and (**d**) d-spacing of CeO_2/NiO nanocomposite.

FTIR spectrum of CeO_2/NiO nanocomposite in the range of 400–4400 cm^{-1} is shown in Figure 6. Here we observed multiple peaks corresponding to bond stretching and bond vibrations of metal oxides.

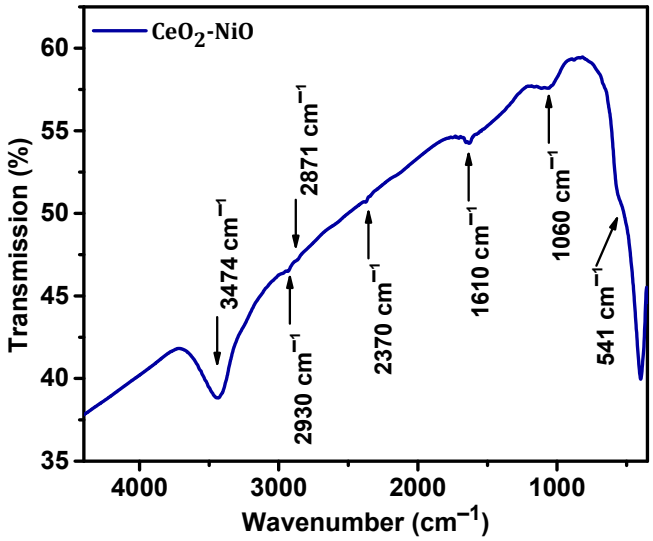

Figure 6. FTIR spectrum of CeO_2/NiO nanocomposite.

A significant peak centered at 404 cm^{-1} the characteristic peak corresponding to the stretching vibration of the Ni-O bond in NiO present in this nanocomposite [25]. The same kind of observation was made by Korosec and Bukovec at a slightly higher wave number i.e., 443 cm^{-1} [26]. The adjacent peak centered at 541 cm^{-1} which was attributed to the characteristic stretching of the Ce-O bond and thus confirmed the presence of CeO_2 [27]. The peaks appearing at 3474 cm^{-1} and 1610 cm^{-1} originated from the bond stretching

and bond bending of H_2O [28]. Other absorption peaks appearing at 2345 and 1618 cm^{-1} verified the presence of metal oxide bonds [29].

Figure 7 depicts the Raman scattering spectrum of the prepared nanocomposite of CeO_2/NiO. It is clear in the figure that there are two well-defined and sharp peaks at 556 cm^{-1} and 540 cm^{-1} in the spectra. For the fluorite cubic structure of ceria, the characteristic peak was observed at 556 cm^{-1} that was sharp-intense. While the other low-intense peak observed at 540 cm^{-1} corresponded to the NiO. These obtained peaks in the Raman spectra were in accordance with the already reported peaks in the literature [30]. These characteristic peaks were also in accordance with the peaks obtained in FTIR spectra.

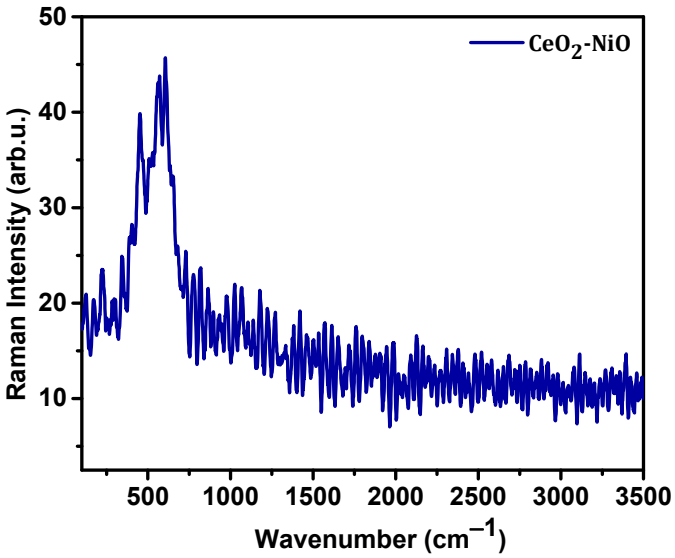

Figure 7. Raman spectrum of CeO_2/NiO nanocomposite.

The XPS analysis could be used to determine the presence of different elements and their oxidation states. The XPS spectrum of this nanocomposite is shown in Figure 8. Figure 8a shows the survey spectrum of the whole nanocomposite while Figure 8b–d reveals the spectrum of O1s, Ni2p, and Ce3d respectively. In O1s, three peaks were observed at 528, 531, and 534 eV (Figure 8b). In the oxygen profile, we had three overlapping peaks which were due to the presence of oxygen from CeO_2 as well as from NiO. The most intense peak appeared at 531 eV [31]. Two peaks of Ni appeared at 855 eV and 861 eV (Figure 8c). Similarly, Figure 8d shows the photoelectron peaks of Ce-3d. The peaks in this spectrum were a little ambiguous not only because of the multi-oxidation states of Ce but also due to the hybridization of 4f of Ce with 2p of oxygen atoms. This hybridization leads to the splitting of Ce-peaks into multiple peaks. However, there was no peak corresponding to Ce_2O_3 in this spectrum [32]. In order to determine the specific surface area and pore volume, we performed the BET analysis which showed that the synthesized electrode material had 21.1817 g/m^2 specific surface area while BJH exposed the value of pore volume to be 0.076 cm^3/g during adsorption which increased to 0.095 cm^3/g during the desorption process.

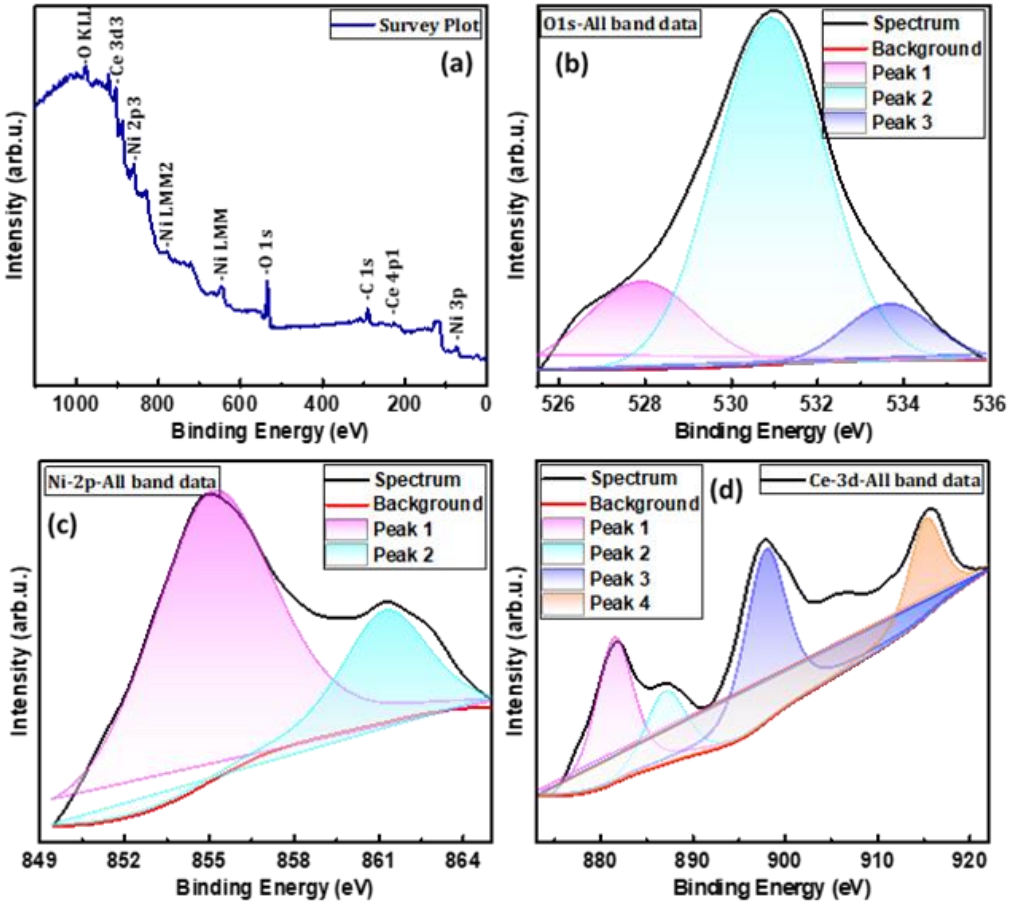

Figure 8. (**a**) Survey spectrum of CeO_2/NiO nanocomposite, XPS spectra of (**b**) O1s, (**c**) Ni2p, and (**d**) Ce3d.

In order to explore the electrochemical performance of this nanocomposite as an electrode material, the CV measurement was carried out. The CV loops of CeO_2/NiO nanocomposite were at different scan rates i.e., 0.005, 0.01, 0.05, and 0.1 V/s in the potential window of 0–0.5 V, as shown in Figure 9a. The charge stored in the material was measured from the area of CV loops. A broader reduction peak appearing at ~0.4V was attributed to the oxidation of NiO which clearly revealed the pseudocapacitive behavior of this nanocomposite. A sudden increase in current values could be observed which may be due to oxidation of anions present in the electrolyte. The same kind of observation had been reported recently by Schiavi et al., 2020 [33,34]. The values of specific capacitances (C_s) could be measured using the formula

$$C_s = A/2\Delta V \times \nu \times m \quad (1)$$

Here, A is the area enclosed by the CV curve, ΔV is the potential window, m is the mass of the electrode, and ν is the scan rate. Table 1 comprises the values of C_s of this nanocomposite at different scan rates. It is obvious from this table that specific capacitance decreased with the increase of scan rates. This decrease of C_s with increasing scan rate was attributed to the decrease of contact time of charges with the electrode. Figure 9b shows the galvanostatic charge-discharge (GCD) curve of the synthesized nanocomposite at various current densities.

Table 1. Calculated values of specific capacitance of CeO_2/NiO nanocomposites at different scan rates.

Area (VA)	Scan Rate (V/s)	Potential Window (V)	Mass (g)	Specific Capacitance (F/g)
8.24×10^{-6}	0.005	0.5	0.001	1.6478
1.19×10^{-5}	0.01	0.5	0.001	1.1893
3.79×10^{-5}	0.05	0.5	0.001	0.7571
6.32×10^{-5}	0.1	0.5	0.001	0.6322

By observing the discharge time from these GCD curves, the C_s, energy density (E), and power density (P) were calculated using the following relations [35–37].

$$E = 1/2C_s\ (\Delta V)^2 \quad (2)$$

$$P = E/(\Delta t) \quad (3)$$

Here, ΔV is the change in potential and Δt is the discharge time. The calculated values of C_s, E, and P at different current densities are summarized in Table 2.

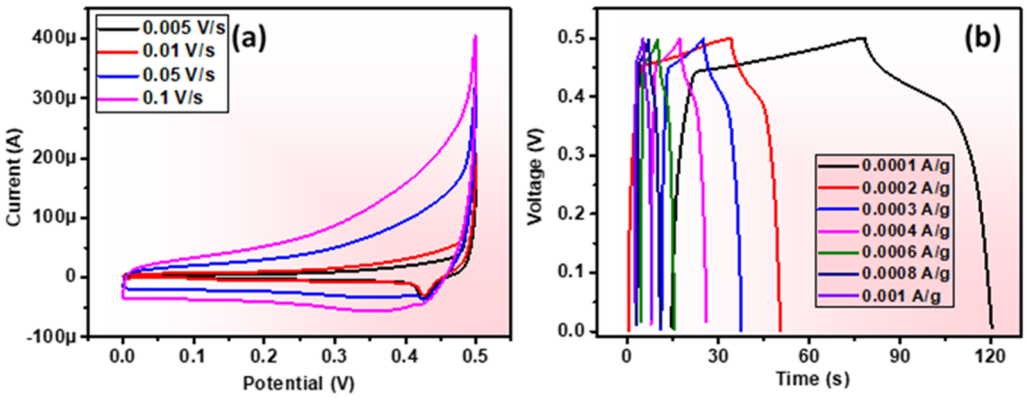

Figure 9. (**a**) CV curves and (**b**) GCD curves of CeO_2/NiO nanocomposite.

Table 2. Calculation of specific capacitance, energy density, and power density of CeO_2/NiO nanocomposites.

Current Density (A/g)	Discharge Time (s)	Potential Drop (V)	Specific Capacitance (mF/g)	Energy Density (mF/g*V^2)	Power Density (mF/s.g*V^2)
1×10^{-4}	42.09	0.5	8.418	1.052	0.025
2×10^{-4}	16.44	0.5	6.576	0.822	0.05
3×10^{-4}	12.83	0.5	7.698	0.962	0.075
4×10^{-4}	8.87	0.5	7.096	0.887	0.1
6×10^{-4}	5.51	0.5	6.612	0.826	0.15
8×10^{-4}	3.81	0.5	6.096	0.726	0.20
1×10^{-3}	2.91	0.5	2.962	0.229	0.0786

In order to have more insight, electrochemical impedance spectroscopy was performed which could provide a quantitative value of resistance offered by the electrolyte and electrode to the charge transfer. An EIS plot of this nanocomposite is shown in Figure 10.

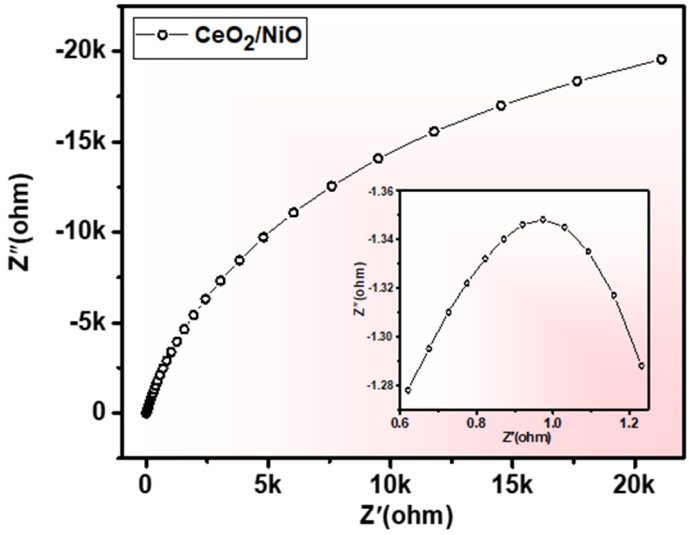

Figure 10. Nyquist plot of CeO_2/NiO nanocomposite.

Generally, the EIS plots represented a slop line in low-frequency regime and semicircular arc in high-frequency regime. Usually, the semicircle in the high-frequency region determines the solution/electrolyte resistance (R_s) while the arc in the low frequency helps to determine the capacitive nature of the material which is quantified by the Warburg coefficient (W). In the present study, we could see the semicircle in the high-frequency region which is represented in the inset of Figure 10. The diameter of this semicircle was 0.5 Ω which determined the resistance of electrolyte. Furthermore, the value of charge transfer resistance could also be estimated from the semicircle in the low-frequency region. For better performance of the electrode material, it should have as low resistance as possible. In previous literature, the minimum reported value of charge transfer resistance is 1.2 Ω, however, in this case, we obtained the minimum value of 0.5 Ω. The comparison of the present work with the literature is given in Table 3 [38–41].

Table 3. Comparison of the present study with the literature.

Composition	Synthesis Method	Reported Year	Charge Transferred Resistance (Ω)	Reference
RGO/β-$Ni(OH)_2$/CeO_2	Hydrothermal	2020	1.99	[38]
$YMnO_3$/CeO_2	sonochemistry	2020	320	[39]
carbon/CeO_2	polymer pyrolysis method	2018	1.2	[40]
CeO_2/NiO	Hydrothermal	2018	1.9	[41]
CeO_2/NiO	Hydrothermal		0.4	This work

4. Conclusions

In nutshell, we synthesized CeO_2/NiO nanocomposite via the hydrothermal route to explore its electrochemical performance as an electrode material for supercapacitor applications. First of all, the presence of both CeO_2 and NiO phases was identified from its structural analysis. Then morphology and composition verification was carried out using SEM and EDX analysis. Polycrystalline nature with crystallites of bipyramid shape was examined through TEM images. FTIR, Raman, and XPS analysis also supported the formation of CeO_2/NiO nanocomposite. Calculated values of specific capacitance, energy density, and power density exposed that CeO_2/NiO nanocomposite has superior electrochemical performance as compared to pure ceria or nickel oxide.

Author Contributions: Data curation, H.A.A.-A. and N.B.; Investigation, N.A.; Methodology, N.A.; Project administration, F.A.A.; Resources, A.A.A.; Software, A.A.A.; Validation, H.A.A.-A.; Writing—original draft, G.M.M.; Writing—review & editing, N.A. and F.A.A. All authors have read and agreed to the published version of the manuscript.

Funding: The authors extend their appreciation to the Deanship of Scientific Research at King Saud University for funding this work through Research Group No. RGP-1438-040.

Institutional Review Board Statement: Not applicable.

Informed Consent Statement: Not applicable.

Data Availability Statement: Data sharing not applicable.

Conflicts of Interest: The authors declare no conflict of interest.

References

1. Zhao, X.; Mao, L.; Cheng, Q.; Li, J.; Liao, F.; Yang, G.; Xie, L.; Zhao, C.; Chen, L. Two-dimensional Spinel Structured Co-based Materials for High Performance Supercapacitors: A Critical Review. *Chem. Eng. J.* **2020**, *387*, 124081. [CrossRef]
2. Yi, T.F.; Wei, T.T.; Mei, J.; Zhang, W.; Zhu, Y.; Liu, Y.G.; Luo, S.; Liu, H.; Lu, Y.; Guo, Z. Approaching High-Performance Supercapacitors via Enhancing Pseudocapacitive Nickel Oxide-Based Materials. *Adv. Sustain. Syst.* **2020**, *4*, 1900137. [CrossRef]
3. Huang, C.; Hao, C.; Zheng, W.; Zhou, S.; Yang, L.; Wang, X.; Zhu, L. Synthesis of polyaniline/nickel ox-ide/sulfonated graphene ternary composite for all-solid-state asymmetric supercapacitor. *Appl. Surf. Sci.* **2020**, *505*, 144589. [CrossRef]
4. Raghavendra, K.V.G.; Vinoth, R.; Zeb, K.; Gopi, C.V.M.; Sambasivam, S.; Kummara, M.R.; Kim, H.J. An in-tuitive review of supercapacitors with recent progress and novel device applications. *J. Energy Storage* **2020**, *31*, 101652. [CrossRef]
5. Chime, U.K.; Nkele, A.C.; Ezugwu, S.; Nwanya, A.C.; Shinde, N.; Kebede, M.; Ejikeme, P.M.; Maaza, M.; Ezema, F.I. Recent progress in nickel oxide-based electrodes for high-performance supercapacitors. *Curr. Opin. Electrochem.* **2020**, *21*, 175–181. [CrossRef]
6. Liu, H.; Liu, X.; Wang, S.; Liu, H.K.; Li, L. Transition metal based battery-type electrodes in hybrid supercapacitors: A review. *Energy Storage Mater.* **2020**, *28*, 122–145. [CrossRef]
7. Oloore, L.E.; Gondal, M.A.; Popoola, A.J.; Popoola, I. Pseudocapacitive contributions to enhanced electrochemical energy storage in hybrid perovskite-nickel oxide nanoparticles composites electrodes. *Electrochim. Acta* **2020**, *361*, 137082. [CrossRef]
8. Padmanathan, N.; Selladurai, S. Electrochemical capacitance of porous NiO–CeO_2 binary oxide synthesized via sol–gel technique for supercapacitor. *Ionics* **2013**, *20*, 409–420. [CrossRef]
9. Karuppaiah, M.; Sakthivel, P.; Asaithambi, S.; Murugan, R.; Yuvakkumar, R.; Ravi, G. Solvent dependent mor-phological modification of micro-nano assembled Mn2O3/NiO composites for high performance supercapacitor applications. *Ceram. Int.* **2019**, *45*, 4298–4307. [CrossRef]
10. Xie, A.; Tao, F.; Li, T.; Wang, L.; Chen, S.; Luo, S.; Yao, C. Graphene-cerium oxide/porous polyaniline composite as a novel electrode material for supercapacitor. *Electrochim. Acta* **2018**, *261*, 314–322. [CrossRef]
11. Maheswari, N.; Muralidharan, G. Hexagonal CeO_2 nanostructures: An efficient electrode material for supercapac-itors. *Dalton Trans.* **2016**, *45*, 14352–14362. [CrossRef] [PubMed]
12. Li, T.; Liu, H. A simple synthesis method of nanocrystals CeO_2 modified rGO composites as electrode materials for supercapacitors with long time cycling stability. *Powder Technol.* **2018**, *327*, 275–281. [CrossRef]
13. Sivasakthi, P.; Bapu, G.R.; Murugavel, K.; Mohan, S. Facile method of pulse electrodeposited NiO-CeO_2Sm doped nanocomposite electrode on copper foam for supercapacitor application. *J. Alloys Compd.* **2017**, *709*, 240–247. [CrossRef]
14. Deng, D.; Chen, N.; Li, Y.; Xing, X.; Liu, X.; Xiao, X.; Wang, Y. Cerium oxide nanoparticles/multi-wall carbon nanotubes composites: Facile synthesis and electrochemical performances as supercapacitor electrode materials. *Phys. E Low Dimens. Syst. Nanostruct.* **2017**, *86*, 284–291. [CrossRef]
15. Ahmad, N.; Alam, M.; Wahab, R.; Ahmad, J.; Ubaidullah, M.; Ansari, A.A.; Alotaibi, N.M. Synthesis of NiO–CeO_2 nanocomposite for electrochemical sensing of perilous 4-nitrophenol. *J. Mater. Sci. Mater. Electron.* **2019**, *30*, 17643–17653. [CrossRef]
16. Ahmad, N.; Umar, A.; Kumar, R.; Alam, M. Microwave-assisted synthesis of ZnO doped CeO_2 nanoparticles as potential scaffold for highly sensitive nitroaniline chemical sensor. *Ceram. Int.* **2016**, *42*, 11562–11567. [CrossRef]
17. Ansari, A.A.; Labis, J.; Alam, M.; Ramay, S.M.; Ahmad, N.; Mahmood, A. Influence of copper ion doping on structural, optical and redox properties of CeO_2 nanoparticles. *J. Electroceram.* **2016**, *36*, 150–157. [CrossRef]
18. Xiong, S.; Jiang, S.; Wang, J.; Lin, H.; Lin, M.; Weng, S.; Chen, J. A high-performance hybrid supercapacitor with NiO derived NiO@ Ni-MOF composite electrodes. *Electrochim. Acta* **2020**, 135956. [CrossRef]
19. Zhang, H.; Gu, J.; Tong, J.; Hu, Y.; Guan, B.; Hu, B.; Wang, C. Hierarchical porous MnO_2/CeO_2 with high per-formance for supercapacitor electrodes. *Chem. Eng. J.* **2016**, *286*, 139–149. [CrossRef]
20. Ramachandran, R.; Zhao, C.; Rajkumar, M.; Rajavel, K.; Zhu, P.; Xuan, W.; Wang, F. Porous nickel oxide mi-crosphere and Ti3C2Tx hybrid derived from metal-organic framework for battery-type supercapacitor electrode and non-enzymatic H_2O_2 sensor. *Electrochim. Acta* **2019**, *322*, 134771. [CrossRef]

21. Manibalan, G.; Murugadossd, G.; Thangamuthu, R.; Ragupathy, P.; Kumar, M.R.; Kumar, R.M.; Jayavel, R. High Electrochemical Performance and Enhanced Electrocatalytic Behavior of a Hydrothermally Synthesized Highly Crystalline Heterostructure CeO_2@NiO Nanocomposite. *Inorg. Chem.* **2019**, *58*, 13843–13861. [CrossRef] [PubMed]
22. Racik, K.M.; Guruprasad, K.; Mahendiran, M.; Madhavan, J.; Maiyalagan, T.; Raj, M.V.A. Enhanced electro-chemical performance of MnO_2/NiO nanocomposite for supercapacitor electrode with excellent cycling stability. *J. Mater. Sci. Mater. Electron.* **2019**, *30*, 5222–5232. [CrossRef]
23. Manibalan, G.; Murugadoss, G.; Thangamuthu, R.; Ragupathy, P.; Kumar, R.M.; Jayavel, R. Enhanced electro-chemical supercapacitor and excellent amperometric sensor performance of heterostructure CeO_2-CuO nanocomposites via chemical route. *Appl. Surf. Sci.* **2018**, *456*, 104–113. [CrossRef]
24. Bose, S.; Kuila, T.; Mishra, A.K.; Rajasekar, R.; Kim, N.H.; Lee, J.H. Carbon-based nanostructured materials and their composites as supercapacitor electrodes. *J. Mater. Chem.* **2012**, *22*, 767–784. [CrossRef]
25. Purushothaman, K.K.; Muralidharan, G. Nanostructured NiO based all solid state electrochromic device. *J. Sol Gel Sci. Technol.* **2007**, *46*, 190–194. [CrossRef]
26. Korošec, R.C.; Bukovec, P. The role of thermal analysis in optimization of the electrochromic effect of nickel oxide thin films, prepared by the sol–gel method: Part II. *Thermochim. Acta* **2004**, *410*, 65–71. [CrossRef]
27. Kaviyarasu, K.; Manikandan, E.; Nuru, Z.Y.; Maaza, M. Investigation on the structural properties of CeO_2 nano-fibers via CTAB surfactant. *Mater. Lett.* **2015**, *160*, 61–63. [CrossRef]
28. Faisal, M.; Khan, S.B.; Rahman, M.M.; Jamal, A.; Akhtar, K.; Abdullah, M.M. Role of ZnO-CeO_2 nanostructures as a photo-catalyst and chemi-sensor. *J. Mater. Sci. Technol.* **2011**, *27*, 594–600. [CrossRef]
29. Tian, J.; Shao, Q.; Dong, X.; Zheng, J.; Pan, D.; Zhang, X.; Guo, Z. Bio-template synthesized NiO/C hollow mi-crospheres with enhanced Li-ion battery electrochemical performance. *Electrochim. Acta* **2018**, *261*, 236–245. [CrossRef]
30. Wu, W.; Qi, W.; Zhao, Y.; Tang, X.; Qiu, Y.; Su, D.; Fan, H.; Wang, G. Hollow CeO_2 spheres conformally coated with graphitic carbon for high-performance supercapacitor electrodes. *Appl. Surf. Sci.* **2019**, *463*, 244–252. [CrossRef]
31. Reddy, B.M.; Khan, A.; Yamada, Y.; Kobayashi, T.; Loridant, S.; Volta, J.-C. Surface Characterization of CeO_2/$SiO_2$and V_2O_5/CeO_2/SiO_2Catalysts by Raman, XPS, and Other Techniques. *J. Phys. Chem. B* **2002**, *106*, 10964–10972. [CrossRef]
32. Oskueyan, G.; Lakouraj, M.M.; Mahyari, M. Nitrogen and sulfur Co-Doped graphene quantum dots decorated CeO_2 nanoparticles/polyaniline: As high efficient hybrid supercapacitor electrode materials. *Electrochim. Acta* **2019**, *299*, 125–131. [CrossRef]
33. Schiavi, P.G.; Altimari, P.; Marzolo, F.; Rubino, A.; Zanoni, R.; Pagnanelli, F. Optimizing the structure of Ni–Ni (OH) 2/NiO core-shell nanowire electrodes for application in pseudocapacitors: The influence of metallic core, Ni (OH) 2/NiO ratio and nanowire length. *J. Alloys Compd.* **2020**, 157718. [CrossRef]
34. Schiavi, P.G.; Altimari, P.; Zanoni, R.; Pagnanelli, F. Full recycling of spent lithium ion batteries with production of core-shell nanowires//exfoliated graphite asymmetric supercapacitor. *J. Energy Chem.* **2020**, *58C*, 336–344. [CrossRef]
35. Maheswari, N.; Muralidharan, G. Supercapacitor behavior of cerium oxide nanoparticles in neutral aqueous elec-trolytes. *Energy Fuels* **2015**, *29*, 8246–8253. [CrossRef]
36. Kumar, R.; Agrawal, A.; Nagarale, R.K.; Sharma, A. High Performance Supercapacitors from Novel Metal-Doped Ceria-Decorated Aminated Graphene. *J. Phys. Chem. C* **2016**, *120*, 3107–3116. [CrossRef]
37. Araújo, A.J.M.; Silva, V.D.; Sousa, A.R.; Grilo, J.P.; Simões, T.A.; Macedo, D.A.; Nascimento, R.M.; Paskocimas, C.A. Battery-like behavior of Ni-ceria based systems: Synthesis, surface defects and electrochemical assessment. *Ceram. Int.* **2019**, *45*, 7157–7165. [CrossRef]
38. Godlaveeti, S.K.; Maseed, H.; Reddy, S.A.; Nagireddy, R.R. Electrochemical performance of ternary RGO/β-$Ni(OH)_2$/CeO_2 composite in addition with different metal oxides for supercapacitor application. *Adv. Nat. Sci. Nosci. Nanotechnol.* **2020**, *11*, 025021. [CrossRef]
39. Wang, Y.; Tian, H. Study on the construction of $YMnO_3$/CeO_2 composite photocatalyst heterostructure and photo-catalytic degradation of methyl red. *Optik* **2020**, *201*, 163524. [CrossRef]
40. Phokha, S.; Hunpratub, S.; Usher, B.; Pimsawat, A.; Chanlek, N.; Maensiri, S. Effects of CeO_2 nanoparticles on electrochemical properties of carbon/CeO_2 composites. *Appl. Surf. Sci.* **2018**, *446*, 36–46. [CrossRef]
41. Phokha, S.; Hunpratub, S.; Chanlek, N.; Sonsupap, S.; Maensiri, S. Synthesis, characterization and electrochemical performance of carbon/Ni-doped CeO_2 composites. *J. Alloys Compd.* **2018**, *750*, 788–797. [CrossRef]